Three-Dimensional Printed Polymethylmethacrylate Casting Molds for Posterior Fossa Reconstruction in the Surgical Treatment of Chiari I Malformation

Pijpker, Peter A. J.; Wagemakers, Michiel; Kraeima, Joep; Vergeer, Rob A.; Kuijlen, Jos M. A.; Groen, Rob J. M.

Published in:
World neurosurgery

DOI:
10.1016/j.wneu.2019.05.191

Publication date:
2019

Accepted Manuscript

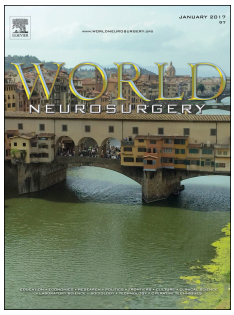

3D-printed PMMA casting molds for posterior fossa reconstruction in the surgical treatment of Chiari I malformation: technical note and illustrative cases

Peter A.J. Pijpker, MSc, Michiel Wagemakers, MD, PhD, Joep Kraeima, MSc, Rob A. Vergeer, MD, Jos M.A. Kuijlen, MD, PhD, Rob J.M. Groen, MD, PhD

PII: S1878-8750(19)31468-8

DOI: https://doi.org/10.1016/j.wneu.2019.05.191

Reference: WNEU 12488

To appear in: *World Neurosurgery*

Received Date: 29 March 2019

Revised Date: 21 May 2019

Accepted Date: 22 May 2019

Please cite this article as: Pijpker PAJ, Wagemakers M, Kraeima J, Vergeer RA, Kuijlen JMA, Groen RJM, 3D-printed PMMA casting molds for posterior fossa reconstruction in the surgical treatment of Chiari I malformation: technical note and illustrative cases, *World Neurosurgery* (2019), doi: https://doi.org/10.1016/j.wneu.2019.05.191.

3D-printed PMMA casting molds for posterior fossa reconstruction in the surgical treatment of Chiari I malformation: technical note and illustrative cases.

Peter A.J. Pijpker [1]; M. Wagemakers [1]; J. Kraeima [2]; R.A. Vergeer [1]; J.M.A. Kuijlen [1]; R.J.M. Groen [1]

[1] University of Groningen, University Medical Center Groningen, Department of Neurosurgery, Groningen, The Netherlands
[2] University of Groningen, University Medical Center Groningen, Department of Oral and Maxillofacial Surgery, Groningen, The Netherlands

Corresponding author:
Peter A.J. Pijpker, MSc
University of Groningen, University Medical Center Groningen, Department of Neurosurgery
Staff Neurosurgery AB71
PO BOX 30.001, 9700 RB Groningen (NL)
p.a.j.pijpker@umcg.nl

Key Words: 3D printing; 3D surgery; Virtual surgical planning; Templates; Chiari malformation type 1; Cranioplasty

Running Title: 3D-printed molds for reconstruction after Chiari decompression surgery.

Abstract word count: 162
Text word count (ex abstract): 2903
Number of references: 23
Number of tables and/or Figures: 8
Number of videos: 1

Declarations of interest: none
There are no sources of funding.

Structured Abstract

Objective: To describe a new method for cranial reconstruction after posterior fossa craniectomy in the surgical treatment of Chiari 1 Malformation, through a technical note and by presenting three illustrative cases.

Methods and materials: A virtual surgical planning workflow was established for planning of the posterior fossa decompression, the design of the suboccipital reconstruction, and for manufacturing of a 3D-printed PMMA casting mold. The casting accuracy was assessed by conducting a phantom experiment and clinical data was provided by means of three illustrative cases.

Results: The accuracy of implant fabrication was found to be excellent, particularly when the PMMA is introduced into the mold in a malleable state. In all three clinical cases the implants were fabricated and positioned with success. Postoperative analysis revealed that accurate placement was achieved, with only minor deviation compared to the preoperative plan.

Conclusions: 3D virtual surgical planning provide feasible tools both for planning of the posterior fossa decompression and to intraoperatively fabricate accurate patient-specific suboccipital cranioplasties.

1. Introduction

The Chiari 1 malformation (CM1) is a common disorder of the craniovertebral junction, traditionally defined as downward displacement of the cerebellar tonsils through the foramen magnum.[1] There is a wide range of symptoms and signs associated with CM1, including Valsalva-induced head and/or neck pain, brainstem symptoms and syringomyelia. Although the exact etiology of CM1 remains unknown, evidence to date suggests that CM1 is associated with an overcrowded posterior fossa, causing disturbed cerebrospinal fluid (CSF) flow dynamics and tonsillar herniation.[2,3]

A lack of agreement among specialists on the most effective surgical strategy for CM1 has led to many different surgical approaches, ranging from solely posterior fossa decompression (PFD), to PFD with duraplasty and cranioplasty.[4] Although the recent trend in surgery is towards minimally invasive procedures, posterior fossa reconstruction (PFR) is reported to be associated with fewer postoperative complications.[5–7] The rigid cranioplasty is supposed to secure the enlarged cisterna magna from pressure and adhesions of nuchal musculature and from extradural scarring. In a pediatric population, PFR was found to be superior with respect to postoperative CSF leakage and pseudomeningoceles compared to only performing a PFD.[5]

It is reported that many CM1 recurrences may be due to arachnoid scarring, intradural adhesions, or dural prolapse [8–10]. Dural prolapse can cause local intradural adhesions, that provoke re-stenosis of the cisterna magna and obstruct the CSF flow. This phenomenon negates the positive effects of PFD surgery and can cause recurrent CM1 symptoms. PFR allows for suturing of the dura to the cranioplasty, i.e. dural tenting, which may contribute to preserving the enlarged cisterna magna. Secondary reconstruction after an initially oversized craniectomy may be useful for those patients who present with postoperative ptosis or slumping[11]

Until to date, there is no standard procedure for reconstruction of the posterior fossa. The different reconstructive techniques include the use of titanium plates, polymethylmethacrylate (PMMA) bone cement, and autologous cranial or iliac bone.[11–14] With the rapid rise of 3D virtual surgical planning (VSP) technology, it is now possible to precisely define and determine the dimensions of craniectomy. This technology might, therefore, be applicable to CM1 patients undergoing PFR surgery. In this study we describe a new approach for using VSP in PFD surgery and creating an accurate patient-specific suboccipital PMMA implant that secures the cisterna magna and facilitates dural tenting.

2. Methods and materials

This paper presents a two-phase approach on the development and assessment of 3D-printed molds for PMMA casting in CM1 surgery. First, a 3D VSP method was developed and validated in a laboratory phantom experiment, to precisely assess the accuracy of PMMA casting. Secondly, we provide clinical data by reporting three illustrative cases that underwent PFD using VSP techniques.

2.1 Phantom experiment

2.1.1 Virtual Surgical Planning

For CM1 patients it seems that the occipital bone is often underdeveloped causing the overcrowding in the posterior fossa.[15] The experiment demanded realistic Chiari occipital bone models, therefore, an available anonymized CT scan was used from a patient who previously underwent PFD surgery. Using threshold based segmentation techniques in Mimics v21 (Materialise, Leuven, Belgium), bone was extracted from CT data (Figure 1a,b,c). The masked bone was then cropped and converted into an unidentifiable representative 3D bone model for the experiment.

The acquired 3D model was imported into 3-matic v12 (Materialise, Leuven, Belgium), which offers a range of tools for computer aided design of the patient-specific implants. First the PFD was virtually performed and the cranioplasty was designed (Figure 1d). This process included several steps, namely, 1) determination of PFD size and shape, 2) virtual craniectomy of the occipital bone, 3) design of a matching implant using a 2mm thick concave dome and a 5mm bone overlay that covers bone around the planned resection, and 4) incorporation of holes for fixation and dural tenting sutures.

The resulting implant model was subsequently used to design a casting mold (Figure 1e). The model was extruded 2mm to obtain a hollow shape that exactly fits the implant model. Then, the holes were incorporated into the mold, which allow for inserting 1.5mm k-wires and thereby cast pre-planned holes in the final plasty. The ultimate model was separated into 2 parts, to obtain the mold's bottom and lid.

The new outline of the occipital bone was carefully checked not to interfere with the C2 spinous process, especially during hyperextension (Figure 1f,g,h). Finally, the molds were 3D-printed in polyamide, a material suitable for autoclave sterilization.

2.1.2 The experiment

To find out the best method for producing the PMMA casted implant we performed two separate tests in which we applied the PMMA in different ways. In the first test, runny-liquid PMMA was applied to the center of the mold using a syringe (Figure 2a). In the second test, we used PMMA that was already polymerized into a malleable dough-like-state, allowing the material to be kneaded into the mold (Figure 2b). The lid of the mold was closed and tightened using surgical clamps with the k-wires inserted (Figure 2c). After the PMMA was completely solidified (approximately 12 minutes following preparation of the mixture), the lid was detached and the implant released by slightly bending the mold's bottom part. A bone rasp was used to smooth out the sharp edges. In order to prevent the PMMA from sticking to the 3D-printed mold, the prints were covered with a thin layer of sterile Vaseline® prior to use.

After the completion of the experiment, a high resolution (0.2mm voxel size) cone-beam CT (CBCT) scan of the implants was acquired to review the casting accuracy and the PMMA porosity . Segmentation techniques, as described above, were used to obtain a 3D model of the final produced outcome. Following manual model alignment of the outcome over the pre-

planned model, 3D model fusion was accomplished using the Iterative Closest Point registration algorithm in 3-matic. A subsequent surface to surface error distance was calculated for each surface point (±50.000 in total) on the corresponding surfaces . This method computes the Euclidean distance to the nearest point on the reference model, that can be used to quantify the casting accuracy.

2.3 Illustrative Cases

2.3.1 Patients

We report 3 consecutive patients that underwent PFD surgery with the use of 3D-plannning and corresponding casting molds. All patients provided informed consent for undergoing PFD by means of 3D-planning and for the publication of their case reports. The 3D-printed molds were used for intraoperative casting of patient-specific suboccipital PMMA implants. Table 1 provides an overview of the cases that underwent surgery using 3D-casted PMMA occipital bone reconstruction. In all of the outlined cases, the purple marked occipital bone represents the 3D-planned PFD. The subsequent occipital reconstruction is marked in green. (Note that the atlas is also displayed in purple).

The first case was a 60-year-old woman who was diagnosed with a CM1 and syringomyelia ranging from C1 to Th11. She presented with common symptoms of CM1, including interscapular pain, and signs of both sensory and motor function loss on the left side of the body. We proposed to her a PFD decompression operation including duraplasty and posterior fossa reconstruction by means of VSP and computer designed PMMA cranioplasty. Additionally, patient-specific craniectomy guiding templates were designed for translation of the VSP towards surgery. Based on our clinical experience and the cerebellar herniation, it was decided to plan an oval-shaped craniectomy measuring 20mm in width and 18mm in length. (table 1)

The second case was a 28-year-old woman with a history of severe tension headaches related to coughing, laughing and forced defecation. Moreover she suffered from a loss of coordination and episodes of sensory disturbances. MR imaging showed a symptomatic CM1 malformation without signs of syrinx cavity. The third case was a 20-year-old male diagnosed with CM1 including a cervicothoracic syringomyelia and atlantoaxial dislocation. He presented to us with symptoms of head and neck pain and sensibility disorders of the right arm and hemithorax.

Similar to the first case, a 3D-planning strategy was deployed for the second and third case, but because of the severity of tonsillar herniation it was decided to extend the decompression width to 25mm, just under the width of the patient's foramen magnum. For all of the above described cases, the craniectomy templates and molds were 3D-printed in polyamide and sterilized by steam autoclave sterilization to be used intra operatively.

2.3.2 Surgical procedure

During surgery, soft tissue was stripped off the squamous part of the occipital bone to allow for a good fit of the craniectomy template (Figure 3a). The resection site was marked by moving the diathermy pencil along the template's inner curvature. The bone marked for resection was thinned using a high-speed round burr, and could be repetitively checked by using the template. Following the completion of the craniectomy, a C1 laminectomy was performed. Then, the dura was incised in a Y-shaped fashion and reduction of the cerebellar tonsils was performed, including the opening of the cisterns to allow free flow of CSF in the craniocervical area. A duraplasty was performed with autologous pericranium, sutured with continuous Ticron® and using fibrin sealant. The patient-specific suboccipital PMMA plasty was casted using similar techniques and materials as previously described. Positioning of the cranioplasty over the defect resulted in the reconstruction of the occipital bone (Figure 3b).

The implant was fixated to the bone by micro screws, and dural tenting was accomplished by suturing the center of the dura to the cranioplasty (Figure 3c,d).

For the first and second case, a postoperative CT-scan was available, allowing to verify the realized position of the suboccipital implant. Superimposition of the preoperative design to the postoperative achieved result was performed to measure the translational and rotational deviation. For the cases with syringomyelia we report the postoperative MR.

3. Results

3.1 Phantom experiment

The final implants produced during the phantom experiments had smooth surfaces, highly similar to the 3D-printed planned-outcome. Upon macroscopic inspection, the implant that was casted using runny-liquid PMMA appeared to have 2 major air bubbles, measuring approximately 2mm in diameter. Using the CBCT scan of the implant, multiple minor internal air bubbles were moreover discovered (Figure 4a). For the malleable PMMA, that was hand kneaded into the mold, the CBCT shows less porosity (Figure 4b). Furthermore, no major air bubbles at the implants surface were discovered. The implants did not show any signs of severe deformations such as bending or fracturing. The surface-to-surface error distribution is visualized in Figure 5. The mean (signed) error distance for the runny-liquid casted and malleable-casted implant was respectively, -0.38mm and -0.09mm, i.e. minimal shrinkage of the implant with respect to the plan. The 95^{th} percentile of the unsigned error distance was 1.80mm for the runny-liquid casted implant and 0.24mm for the malleable-casted implant, i.e. for the malleable-casted implant 95 percent of the surface had an error distance below 0.24mm.

3.2 Clinical results

Successful intraoperative fabrication and placement of the implants using 3D-printed templates and molds was realized in all three cases. No intraoperative complications occurred. The surgeons reported that the implant fit was excellent in all of the cases. Postoperative MR revealed a regression of the syrinx in case 1 and 3 (Figure 6).

The translational error with respect to the planned positions was subdivided into anterior-posterior, left-right, and cranial-caudal displacement parameters. The first case revealed a 0.85mm left displacement, a 2.11mm anterior displacement, and a 0.14mm caudal

displacement (Figure 7). For the second case the displacements were respectively 1.39mm to the left, 0.47mm to posterior, and 0.12mm to caudal. The 3D rotational error analysis for the first case showed a 1.59° clockwise rotation in the axial view, a 2.18° clockwise rotation in the sagittal view, and a 1.45° clockwise rotation in coronal view (Figure 7). For the second case this was respectively, 6.48° axial clockwise, 0.18° sagittal counterclockwise, and 1.58° coronal clockwise.

4. Discussion

This report demonstrates the feasibility of 3D virtual surgical planning techniques for application in CM1 surgery. The presented workflow facilitated (1) accurate 3D planning of the PFD, (2) translation of craniectomy to surgery using patient-specific craniectomy templates, (3) preoperative planning of the occipital reconstruction, (4) accurate intraoperative casting and positioning of a low-cost, patient-specific occipital PMMA implant, and (5) dural tenting using incorporated suture holes.

Although it is reported that occipital reconstruction can help to prevent the frequently reported complications after PFD, little is known about the best reconstructive technique. Traditionally the most simple and direct solution is the use of PMMA, which can be shaped by hand and is fixated to the bone by sutures or screws and plates. However, in literature, modifications were made with regard to material and technique used for the suboccipital reconstruction. Hellar et al. described the use of split-thickness calvarial bone graft, harvested from the occipital region and stacked over the defect so that is forms a concave dome.[16] Takayasu et al. presented a technique that uses a harvested bone flap, which is tailored to fit the occipital defect by modifying the internal crest or placing it inside-out.[14] More recently, the use of perforated titanium plates as occipital cranioplasty are reported.[12,13,17] These plates are available in different sizes and shapes through various manufactures.

To the best of our knowledge, the PMMA casting technique for the application in CM1 surgery, has not been described until now. Although, the use of PMMA casting by 3D-printing techniques is frequently described for cranial reconstruction after decompressive craniectomy. Casting molds were first reported to be used preoperatively, as an impression cavity mold, by kneading the PMMA into the mold.[18] Other studies describe the use of casting molds intraoperatively, for example, by using an impression cavity mold in a sterile bag,[19,20]

or by using 2-part sterilized molds that cast both the inner as well as the outer implant contours.[21–23] In our study, the complete implant was virtually preplanned according to the preoperative CT-scan, which required a 2-part mold. In addition, our method includes a mold that contains k-wire holes, a unique feature that precasts fixation and suture holes.

We found that implant casting is highly accurate, especially when the PMMA is applied in malleable state. This was also confirmed by the good fit the surgeons experienced in the described cases. Unlike a titanium mesh or autologous bone, that is intraoperatively shaped by the surgeon, the PMMA implant casting can be done parallel to the surgical procedure, and therefore might reduce operative time. Conversely, however, the use of VSP requires additional preoperative time (approximately 2-3 hours per case), which should be included into future cost-effectiveness calculations.

The accuracy of implant positioning with respect to the VSP plan was found to be good. Inaccuracies might occur by improper positioning of the craniectomy template on the occipital bone. Since the squamous part of the occipital bone can be relatively flat, finding the proper fit of the template can sometimes be problematic. In particular, improper design may result in the positioning of the templates in an unintended manner. The occipital plane, however, offers some distinct anatomical landmarks that provide stable bony support for the craniectomy template. We therefore advise to use the external occipital crest and the edges of the foramen magnum as reference points in the template to allow for correct positioning.

The present study is intended solely to describe the feasibility of this technology for CM1 surgery and might therefore have some limitations. Currently, due to a lack of consensus about the most adequate size of craniectomy, the sizing of decompression and implant is based on experience rather than supported by quantitative clinical evidence. Moreover, the currently used design is based on a concave oval-shaped dome, but different shapes might be

superior in terms of clinical outcome. Future research should, therefore, study the 3D characteristics of the PFD and the produced implant, which can help to optimize the current workflow and may in future result in improved patient outcome after CM1 surgery.

In conclusion, 3D VSP is a feasible tool for both planning of the posterior fossa decompression and to intraoperatively fabricate accurate patient-specific suboccipital cranioplasties.

References

1. Schijman E. History, anatomic forms, and pathogenesis of Chiari I malformations. *Child's Nerv Syst*. 2004;20(5):323-328. doi:10.1007/s00381-003-0878-y.

2. Shaffer N, Martin B, Loth F. Cerebrospinal fluid hydrodynamics in type I Chiari malformation. *Neurol Res*. 2011;33(3):247-260.

3. Bunck AC, Kroeger JR, Juettner A, et al. Magnetic resonance 4D flow analysis of cerebrospinal fluid dynamics in Chiari I malformation with and without syringomyelia. *Eur Radiol*. 2012;22(9):1860-1870.

4. Munshi I, Frim D, Stine-Reyes R, Weir BKA, Hekmatpanah J, Brown F. Effects of posterior fossa decompression with and without duraplasty on chiari malformation-associated hydromyelia. *Neurosurgery*. 2000;46(6):1384-1390. doi:10.1097/00006123-200006000-00018.

5. Gnanalingham KK, Lafuente J, Thompson D, Harkness W, Hayward R. Surgical procedures for posterior fossa tumors in children: does craniotomy lead to fewer complications than craniectomy? *J Neurosurg*. 2002;97(4):821-826.

6. Schessel DA, Rowed DW, Nedzelski JM, Feghali JG. Postoperative pain following excision of acoustic neuroma by the suboccipital approach: observations on possible cause and potential amelioration. *Otol Neurotol*. 1993;14(5):491-494.

7. Feghali JG, Elowitz EH. Split calvarial graft cranioplasty for the prevention of headache after retrosigmoid resection of acoustic neuromas. *Laryngoscope*. 1998;108(10):1450-1452.

8. Abla AA, Link T, Fusco D, Wilson DA, Sonntag VKH. Comparison of dural grafts in

Chiari decompression surgery: review of the literature. *J Craniovertebr Junction Spine*. 2010;1(1):29.

9. Rosen DS, Wollman R, Frim DM. Recurrence of symptoms after Chiari decompression and duraplasty with nonautologous graft material. *Pediatr Neurosurg*. 2003;38(4):186-190.

10. Sahuquillo J, Rubio E, Poca M-A, Rovira A, Rodriguez-Baeza A, Cervera C. Posterior fossa reconstruction: a surgical technique for the treatment of Chiari I malformation and Chiari I/syringomyelia complex–preliminary results and magnetic resonance imaging quantitative assessment of hindbrain migration. *Neurosurgery*. 1994;35(5):874-885.

11. Holly LT, Batzdorf U. Management of cerebellar ptosis following craniovertebral decompression for Chiari I malformation. *J Neurosurg*. 2001;94(1):21-26. doi:10.3171/jns.2001.94.1.0021.

12. Udani V, Holly LT, Chow D, Batzdorf U. Posterior fossa reconstruction using titanium plate for the treatment of cerebellar ptosis after decompression for Chiari malformation. *World Neurosurg*. 2014;81(5-6):836-841. doi:10.1016/j.wneu.2013.01.081.

13. Assina R, Meleis AM, Cohen MA, Iqbal MO, Liu JK. Titanium mesh-assisted dural tenting for an expansile suboccipital cranioplasty in the treatment of Chiari 1 malformation. *J Clin Neurosci*. 2014;21(9):1641-1646. doi:10.1016/j.jocn.2014.03.006.

14. Takayasu M, Takagi T, Hara M, Anzai M. A simple technique for expansive suboccipital cranioplasty following foramen magnum decompression for the treatment of syringomyelia associated with Chiari I malformation. *Neurosurg Rev*.

2004;27(3):173-177. doi:10.1007/s10143-004-0338-5.

15. Shoja MM, Ramdhan R, Jensen CJ, Chern JJ, Oakes WJ, Tubbs RS. Embryology of the craniocervical junction and posterior cranial fossa, part I: development of the upper vertebrae and skull. *Clin Anat*. 2018;31(4):466-487.

16. Heller JB, Lazareff J, Gabbay JS, Lam S, Kawamoto HK, Bradley JP. Posterior cranial fossa box expansion leads to resolution of symptomatic cerebellar ptosis following Chiari I malformation repair. *J Craniofac Surg*. 2007;18(2):274-280.

17. Oró JJ, Mueller DM. Posterior fossa decompression and reconstruction in adolescents and adults with the Chiari I malformation. *Neurol Res*. 2011;33(3):261-271.

18. Lee S-C, Wu C-T, Lee S-T, Chen P-J. Cranioplasty using polymethyl methacrylate prostheses. *J Clin Neurosci*. 2009;16(1):56-63.

19. Moser M, Schmid R, Schindel R, Hildebrandt G. Patient-specific polymethylmethacrylate prostheses for secondary reconstruction of large calvarial defects: a retrospective feasibility study of a new intraoperative moulding device for cranioplasty. *J Cranio-Maxillofacial Surg*. 2017;45(2):295-303.

20. Hay JA, Smayra T, Moussa R. Customized polymethylmethacrylate cranioplasty implants using 3-dimensional printed polylactic acid molds: technical note with 2 illustrative cases. *World Neurosurg*. 2017;105:971-979.

21. Kim B-J, Hong K-S, Park K-J, Park D-H, Chung Y-G, Kang S-H. Customized cranioplasty implants using three-dimensional printers and polymethyl-methacrylate casting. *J Korean Neurosurg Soc*. 2012;52(6):541.

22. Morales-Gómez JA, Garcia-Estrada E, Leos-Bortoni JE, et al. Cranioplasty with a low-

cost customized polymethylmethacrylate implant using a desktop 3D printer. *J Neurosurg*. 2018;1(aop):1-7.

23. Guerrini F, Dallolio V, Grimod G, Cesana C, Vismara D, Franzin AB. It Is Time to Reduce Free-Hand Manipulation: Case Report of Our Proposal for an Innovative 1-Step Cranioplasty. *World Neurosurg*. 2017;107:1052-e7.

Figure Legend:

Figure 1 - Overview of the Virtual Surgical Planning workflow for CM1 surgery. Bone segmentation in A) axial, B) sagittal, and C) coronal view. Design of D) implant, and E) casting mold. CT overlays of PFD in yellow and cranioplasty in red, in F) axial, G) sagittal and, H) coronal view.

Figure 2 - A) Runny liquid versus, B) dough-like-state PMMA. C) overview after positioning of the lid and the towel clamps.

Figure 3 - Intraoperative photographs, A) The craniectomy template positioned on the occipital bone to mark the outlines of the craniectomy and to guide the surgical burr. B) After craniectomy and duraplasty, the final cranioplasty is positioned. C) The implant is secured using micro screws. D) Final result including tag-suture for dura tenting. Note that the dural-tenting sutures are indicated by a white arrow.

Figure 4 - Sagittal views of the CBCT scans for, A) the runny-liquid casted implant, and B) malleable-casted implant.

Figure 5 - Results of casting accuracy by means of the error distribution plots. The deviation between the planned and actual result were compared after superimposing the post-procedural 3D model onto the planned cranioplasty model. The superior (upper) and inferior (lower) error distribution plots are displayed for the A) runny-liquid and B) malleable casted PMMA.

Figure 6 - Sagittal view of T2-weighted MR images revealing regression of the syrinx in case 1 and 3. A) Preoperative image of case 1 with tonsillar herniation and an associated syringomyelia. B) Postoperative view after PFD, C1 laminectomy and PFR, demonstrating a

syringomyelia reduction. An overview for the third case is provided in C) preoperative view, and D) the postoperative view. The PMMA implants are indicated by white arrows.

Figure 7 - Analysis of implant position for case 1. Translational and rotational deviation between plan (green) and outcome (red) in the A) axial plane, B) sagittal plane and, C) coronal plane.

Table 1- Patient characteristics

Supplemental Video 1 - Animation video of the 3-dimensional planned posterior fossa decompression and reconstruction.

No.	Age	Sex M/F	3D plan	Dimensions Craniectomy
1	60	F	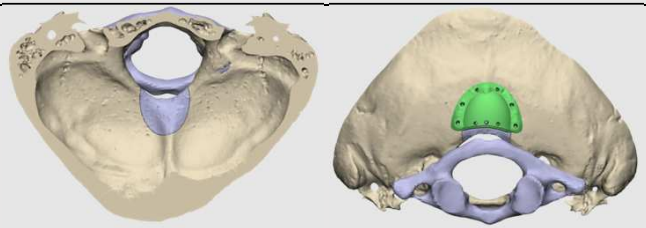	L=18mm W=20mm
2	28	F	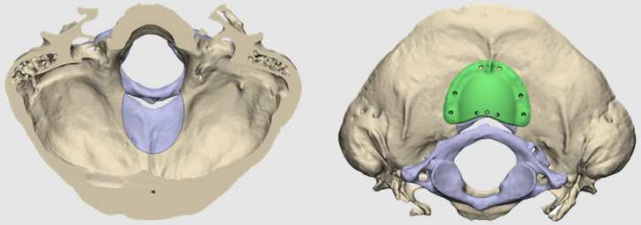	L=21mm W=25mm
3	20	M	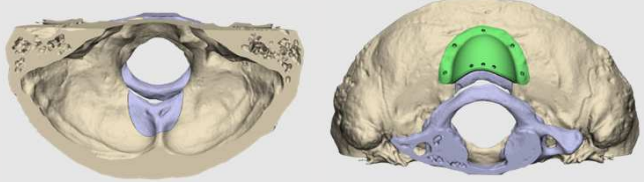	L=24mm W=25mm

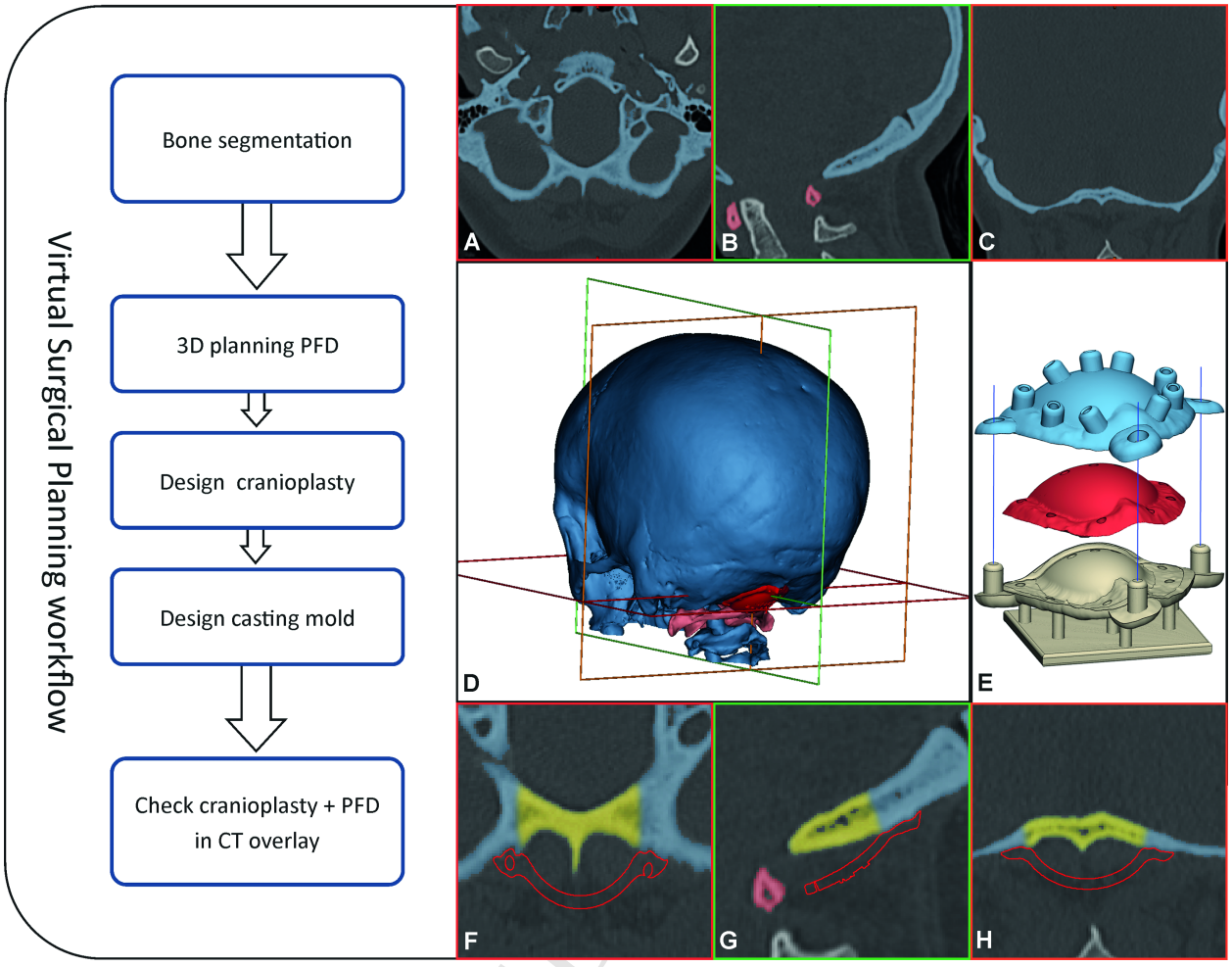
Virtual Surgical Planning workflow
Bone segmentation
3D planning PFD
Design cranioplasty
Design casting mold
Check cranioplasty + PFD in CT overlay
A
B
C
D
E
F
G
H

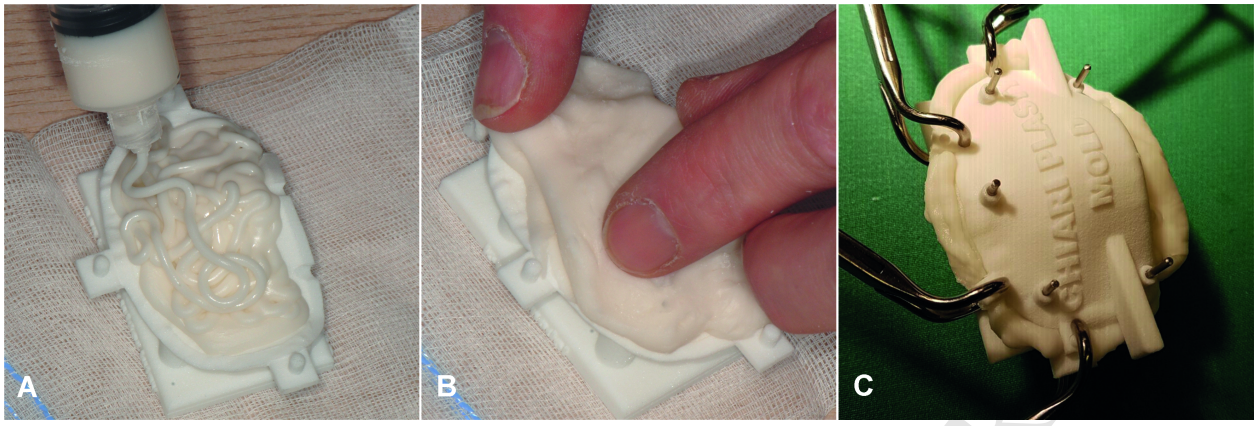

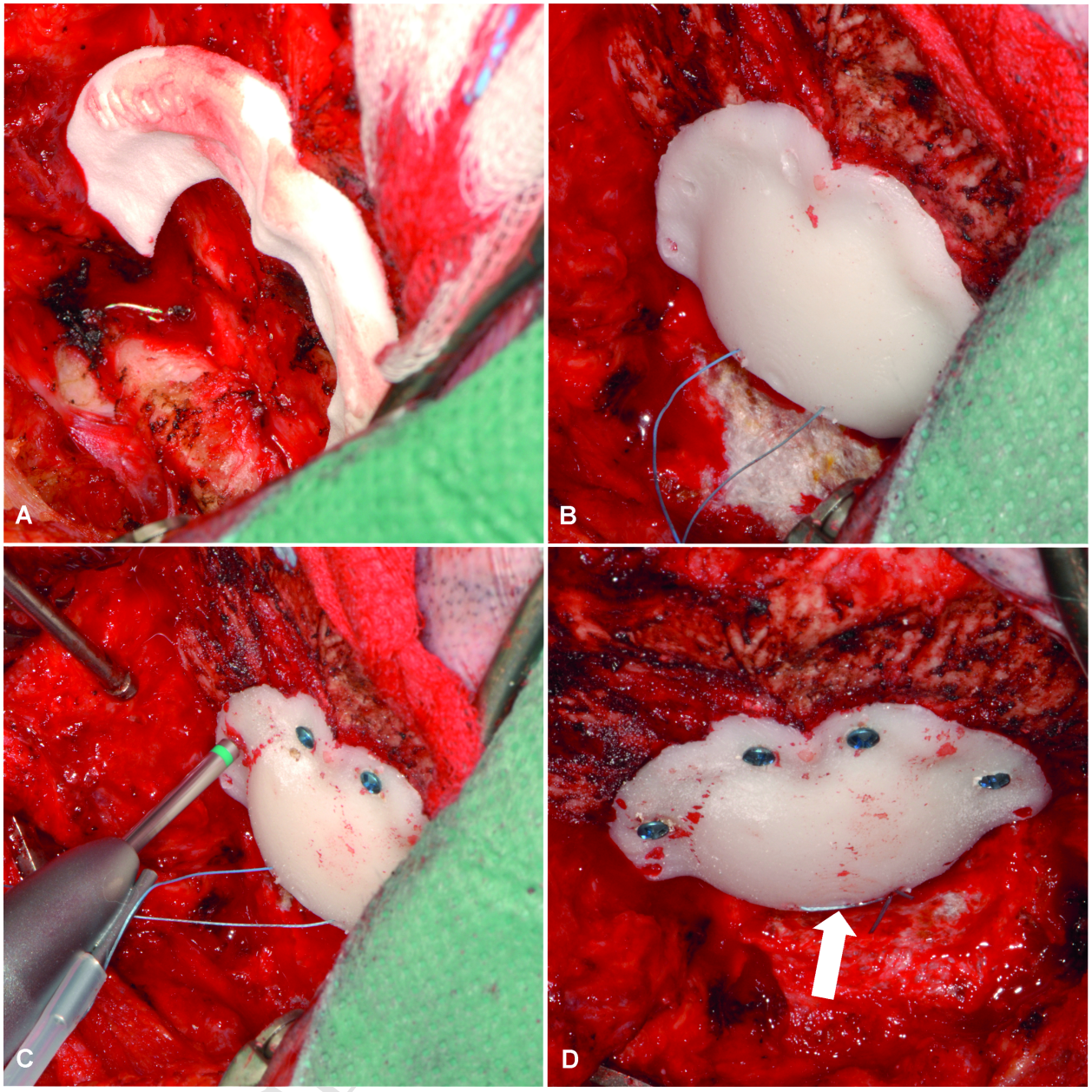

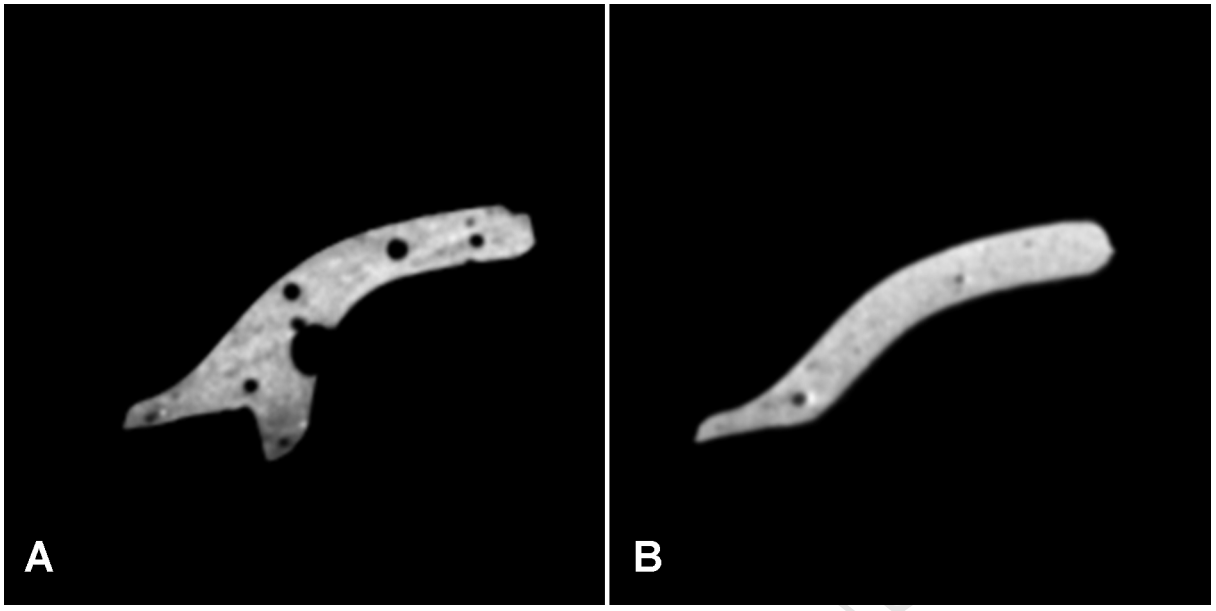

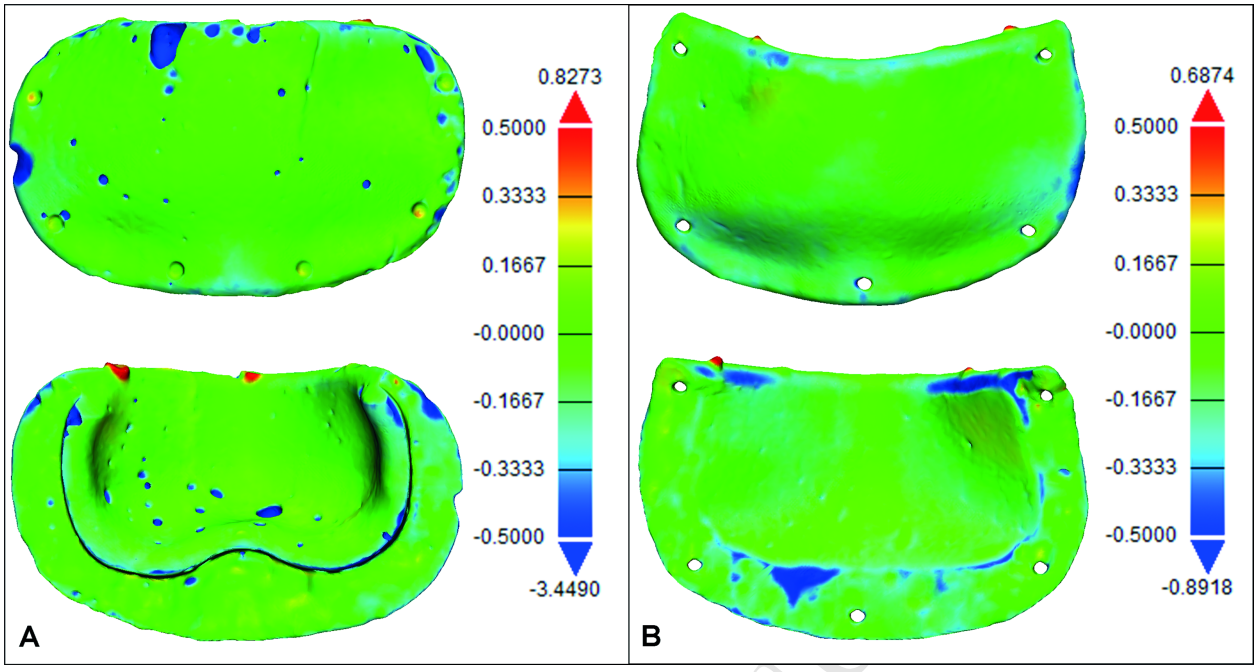

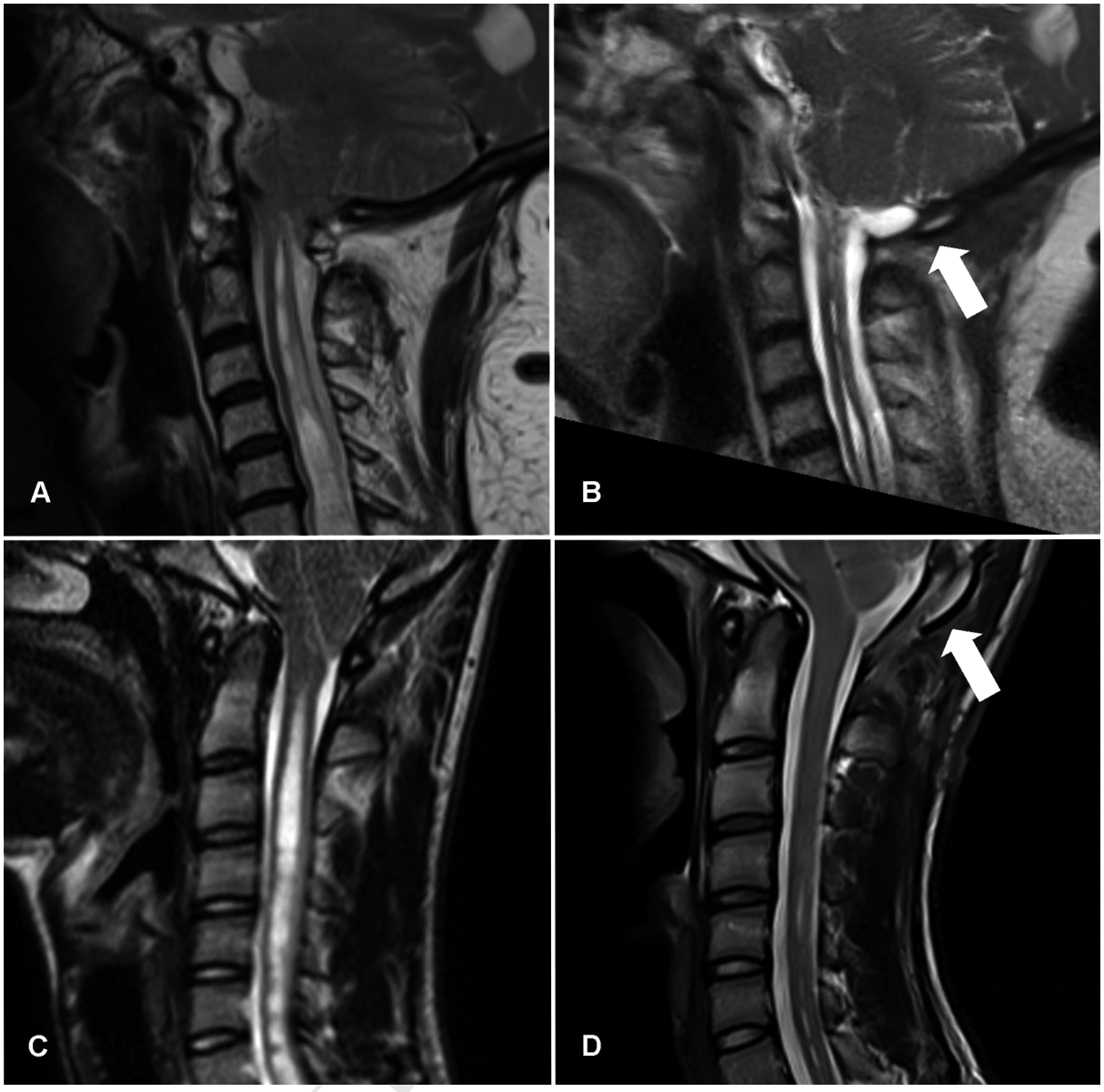

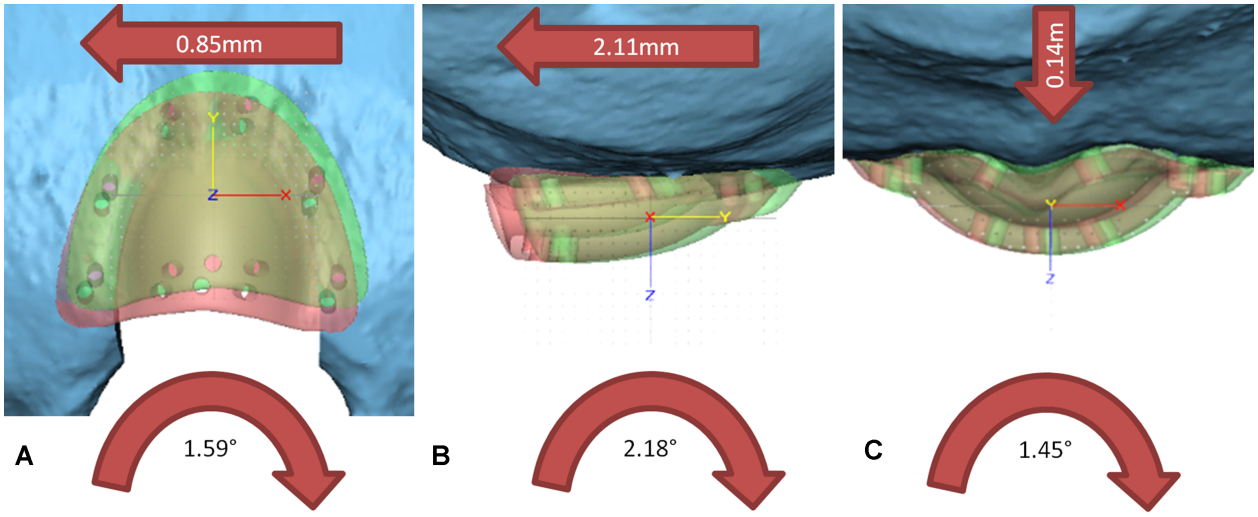

Abbreviations

(3D) Three-Dimensional

(CM1) Chiari Malformation type 1

(CBCT) Cone Beam Computed Tomography

(CT) Computed Tomography

(PFD) Posterior Fossa Decompression

(PFR) Posterior Fossa Reconstruction

(PMMA) Polymethylmethacrylate

(VSP) Virtual Surgical Planning